materials

MDPI

Article

Effect of Contents on the Electrical and Piezoelectric Properties of (1−x)(Bi, Na)TiO_3–x(Ba, Sr)TiO_3 Lead-Free Piezoelectric Ceramics

Seok-Mo Kang [1], Tae Wan Kim [2], Nam-Hoon Kim [3], Sung-Jin Kim [4] and Jung-Hyuk Koh [1,2,*]

[1] School of Electrical and Electronic Engineering, Chung-Ang University, Seoul 06974, Republic of Korea
[2] Department of Intelligent Energy and Industry, Chung-Ang University, Heukseok-ro, Seoul 06974, Republic of Korea
[3] Department of Electrical Engineering, Chosun University, Chosundae-gil, Dong-gu, Gwangju 61452, Republic of Korea
[4] College of Electrical and Computer Engineering, Chungbuk National University, Cheongju 28644, Republic of Korea
* Correspondence: jhkoh@cau.ac.kr; Tel.: +82-2-820-5311

Abstract: In this study, the composition of lead-free piezoelectric ceramics (1−x)($Bi_{0.5}Na_{0.5}$)TiO_3–x($Ba_{0.5}Sr_{0.5}$)TiO_3 with excellent piezoelectric properties was investigated. Crystal analysis and electrical and piezoelectric properties were analyzed according to the content of the BST composition. A phase change from rhombohedral to tetragonal structure was observed in 0.12 BST, and the densest and most uniform microstructure was confirmed in this composition. The dielectric constant increased from 905 to 1692 as the composition of BST increased to 0.12 BST. Afterward, as the composition of BST increased, the permittivity tended to decrease. Additionally, at 0.12 BST, P_r was the highest at 23.34 μC/cm^2. The piezoelectric charge constant (d_{33}) and the electromechanical coupling coefficient (k_p) were 152 pC/N and 0.37, respectively, and showed the highest values at 0.12 BST. Curie temperature (T_m) was analyzed 242 °C at 0.12 BST, the optimal composition. It was confirmed that the characteristics of 0.12 BST were excellent in all conditions. Therefore, it was confirmed that 0.12 BST is the optimal composition for (1−x)BNT–xBST piezoelectric ceramics.

Keywords: piezoelectric materials; lead-free; ceramics; BNT–BST; electrical properties

Citation: Kang, S.-M.; Kim, T.W.; Kim, N.-H.; Kim, S.-J.; Koh, J.-H. Effect of Contents on the Electrical and Piezoelectric Properties of (1−x)(Bi, Na)TiO_3–x(Ba, Sr)TiO_3 Lead-Free Piezoelectric Ceramics. *Materials* **2023**, *16*, 1469. https://doi.org/10.3390/ma16041469

Academic Editor: Georgios C. Psarras

Received: 11 January 2023
Revised: 4 February 2023
Accepted: 7 February 2023
Published: 9 February 2023

1. Introduction

PZT-based piezoelectric ceramics have been widely used as electro-devices due to their excellent piezoelectric properties and high stability [1,2]. However, the use of lead has begun to be regulated because the high content of lead not only hurts the environment but also harms the human body. Accordingly, research on lead-free ceramics has been actively conducted [3]. Various types of ceramics are being studied due to their excellent piezoelectric properties, including (K, Na)NbO_3, $BaTiO_3$, $Bi_{0.5}Na_{0.5}TiO_3$, and BLSF-based ceramics, which are classified as lead-free piezoelectric ceramics [4–6]. Among them, $Bi_{0.5}Na_{0.5}TiO_3$ (BNT) has a high Curie temperature T_c (320 °C), a remnant polarization P_r (38 μC/cm^2), and a high coercive field E_c (7.3 kV/mm) [7]. However, due to the depolarization temperature (T_d) that appears around 185 °C, there is a limit to its use as an actuator. In addition, leakage current is generated due to the volatilization of Bi and Na, which makes the polarization process difficult. In general, BNT materials are not easily polarized at low electric fields, so they have a higher coercive electric field than other piezoelectric ceramics. BNT piezoelectric ceramics exhibit weak thermal values at low electric fields. These large strain values are based on field-induced phase transitions. In particular, Jeong et al. demonstrated that electric field-induced phase transitions can enhance large strains for polycrystalline materials composed of large grains and diastolic matrices. Without coupling any other components, the ternary BNT system exhibits moderate piezoelectric properties. BNT has a rhombohedral perovskite structure with a

piezoelectric charge coefficient of 66 pC/N and an electromechanical coupling coefficient of 21.9%. This material exhibits a high reverse piezoelectric charge factor of 174 pm/V at an electric field of 8 kV/m. However, introducing other components such as Li, Ba, Zr, and K can enhance the piezoelectric properties [8]. Therefore, it is necessary to improve the piezoelectric properties by adding an appropriate dopant [9]. To improve piezoelectric properties, many studies on BNT-based solid solutions have been conducted: such as BNT–BT, BNT–BKT, and BNT–ST [10–14]. BNT–BST materials have recently been studied in various works [15–17]. $Ba_{0.5}Sr_{0.5}TiO_3$ (BST) is proposed as another alternative dopant. Since the unit cell volume of BST is more significant than that of BNT, it is advantageous to improve piezoelectric properties. Further, since BST (1750) has a higher permittivity than BNT (500) and has the same perovskite structure, it affects the improvement of BNT permittivity. This experiment was conducted to analyze the existing composition of BNT–BST. The advantages of the BNT–BST configuration are as follows: First, the relative permittivity of BNT–BST ceramics is slightly higher than that of BNT systems. Additionally, the piezoelectric charge coefficient of the BNT–BST system is also higher than that of the BNT systems. Finally, BNT–BST is a lead-free piezoelectric material.

In this study, BNT–BST piezoelectric ceramics were fabricated in several compositions. Previously, the piezoelectric properties of BNT–BST materials had been analyzed. However, tetragonality was analyzed through 002/200 peak XRD analysis, and the properties of piezoelectric ceramics were studied through microstructure analysis through SEM analysis. In addition, the composition was analyzed and studied in more detail compared to the existing research on BNT–BST ceramics. Therefore, this study analyzed the optimal composition of the BNT-BST ceramic through electrical properties.

2. Materials and Methods

(1−x)BNT–xBST (x = 0.08, 0.10, 0.12, 0.14, 0.16) was fabricated through the conventional sintering method: solid-state reaction. Bi_2O_3 (99.9% purity, Sigma-Aldrich Co., Ltd., Darmstadt, Germany), Na_2CO_3 (99.0% purity, Sigma-Aldrich Co., Ltd., Germany), $BaCO_3$ (99.0% purity, Sigma-Aldrich Co., Ltd., Milan, Italy), $SrCO_3$ (99.9% purity, Sigma-Aldrich Co., Ltd., Italy), and TiO_2 (99.9% purity, High Purity Chemicals, Tokyo, Japan) were used as raw materials. BNT was stoichiometrically weighed out of Bi_2O_3, Na_2CO_3, and TiO_2 and ball-milled with an yttria-stabilized zirconia ball and anhydrous ethyl alcohol for 24 h. Thereafter, it was calcined at 900 °C for 2 h. BST was calcined at 800 °C for 2 h using $BaCO_3$, $SrCO_3$, and TiO_2 in the same way. The calcined BNT and BST powders were weighed by 8, 10, 12, 14, and 16 mol %, mixed, and then ball-milled for 24 h. Thereafter, ethanol was dried at 120 °C, and a PVA binder was added to the sieve to a size of 100 μm to prepare a uniform powder. It was made into discs with a radius of 10 mm through single-axis press molding and sintered at 1200 °C for 3 h. The fabricated specimens were polarized for 30 min in a silicone oil bath under a DC electric field of 4 kV/mm.

The crystal structure of the fabricated BNT–BST ceramics was analyzed by X-ray diffraction (XRD; Rigaku, MiniFlex 600, Tokyo, Japan). The structure of the surface was observed through field-emission scanning electron microscopy (FE-SEM; Carl Zeiss, SIGMA 300, Oberkochen, Germany). The density of manufactured ceramics was measured by the Archimedes method. BNT–BST ceramics were polished and pasted with silver electrodes on both sides to measure the electric properties. The piezoelectric coefficient d_{33} was measured using a d_{33} meter (YE2730A, Manchester, UK). The effective permittivity coefficient (ε_r) according to frequency was measured through an impedance analyzer (Agilent 4294A, Santa Clara, CA, USA). The electromechanical coupling coefficient was calculated through the measured resonant and antiresonant frequencies. Remnant polarization was measured under an alternating electric field of 4 kV/mm at 60 Hz—the Sawyer–Tower method [18]. To obtain the maximum dielectric permittivity temperature (T_m), an impedance analyzer (FLUKE PM6304) was used to obtain the value when the temperature dropped.

3. Results and Discussion

Figure 1 shows the XRD patterns of sintered (1−x)BNT–xBST ceramics. All compositions had a perovskite structure; a secondary phase was not present, such as a pyrochlore phase. As the BST composition increased, it was observed that the peak shifted to a lower angle. This phenomenon is because the lattice parameter increases as the ratio of Ba^{2+} (1.61 Å) and Sr^{2+} (1.44 Å) ions with relatively significant ionic radii increases. (The ionic radii of Bi^{3+} and Na^{+} are 1.40 Å and 1.39 Å, respectively) [19]. It can be inferred from the tolerance factor that small ions occupy the B-site (r < 0.87 Å) and large ions occupy the A-site (r > 0.94 Å) [20]. Considering the cation radii of Ba^{2+} (r = 1.61 Å) and Sr^{2+} (r = 1.44 Å), they tend to enter the A-site of the perovskite structure, which has some effect on the crystal lattice. At the 111 peak, around 40°, it can be seen that the split peaks merge as the composition of BST increases. In addition, it can be seen that the 002 peak around 46° is split when the BST composition is 12 mol % or more. Around x = 0.12, the phase changes from a rhombohedral structure to a tetragonal structure. The lattice constant of ceramics according to the BST composition is shown in Table 1 and was calculated by the following Equations (1) and (2) [21,22]:

$$\frac{1}{d^2_{Rhombohedral}} = \frac{1}{a^2}\frac{\left(h^2+k^2+l^2\right)\sin^2 a + 2(hk+kl+lh)\left(\cos^2 a+\cos a\right)}{1-3\cos^2 a+2\cos^3 a} \quad (1)$$

$$\frac{1}{d^2_{Tetragonal}} = \frac{h^2+k^2}{a^2}+\frac{l^2}{c^2} \quad (2)$$

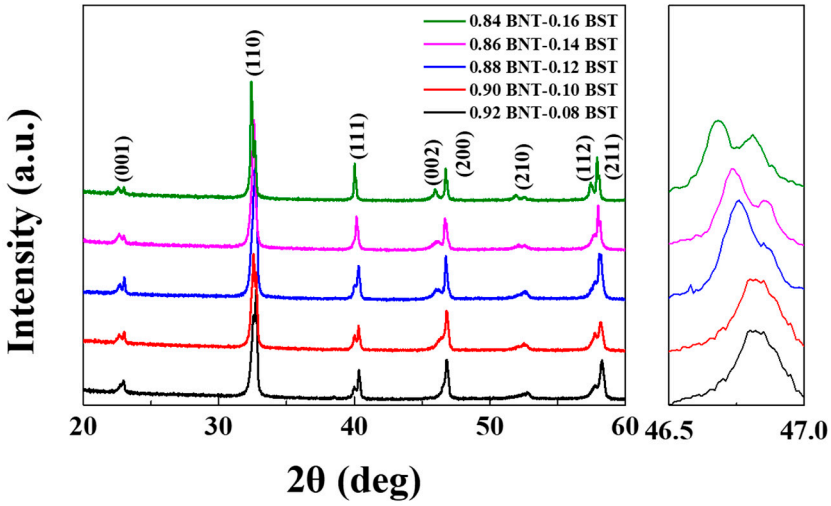

Figure 1. X-ray diffraction of (1−x)BNT–xBST ceramics according to BST content.

Table 1. Lattice constant of (1−x)BNT–xBST ceramics according to BST content.

		0.08 BST	0.10 BST	0.12 BST	0.14 BST	0.16 BST
Crystal Structure		Rhombohedral	Rhombohedral	Tetragonal	Tetragonal	Tetragonal
length	a	3.879 Å	3.879 Å	3.875 Å	3.880 Å	3.886 Å
	c			3.882 Å	3.8789 Å	3.8758 Å
Angle	α	90.2543°	90.067°		90°	

Figure 2 shows the ratio of (200)/(002) for various BST compositions. It was confirmed that the (200)/(002) ratio increased as the BST composition increased to 0.12 BST. In 0.12 BST, the ratio of (200)/(002) was confirmed to be 75.5%, and it was confirmed that the most c-axis

growth was observed. In BST-based piezoelectric ceramics, as the BST content increased, the increase in the (200)/(002) ratio affected the increase in tetragonality. After that, as the content of BST increased, the (200)/(002) ratio seemed to decrease due to two split peaks [23,24]. Therefore, 0.12 BST is expected to have excellent electrical and piezoelectric properties in.

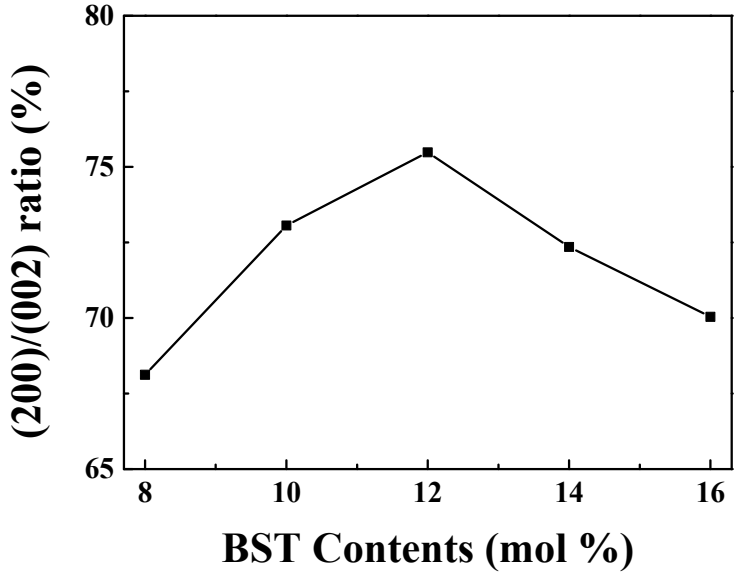

Figure 2. Peak ratio of (200)/(002) in the (1−x)BNT–xBST according to BST content.

Figure 3 shows the FE-SEM images of the (1−x)BNT–xBST ceramics. A dense crystal structure was confirmed in the range of BST composition of $0.08 \leq x \leq 0.12$, as shown in Figure 3a–c. In general, it has been reported that ceramics having a high-density microstructure have improved electrical properties [25]. Generally, ceramics with a dense microstructure are reported to have improved electrical properties [26]. It is known that the average grain size for the composition x = 0.08–0.12 is about 2 μm [27]. The average grain size was 1.82, 1.94, and 1.99 μm in 0.08 BST, 0.10 BST, and 0.12 BST, respectively. In the composition of 0.14 BST, as shown in Figure 3d, the grains were relatively non-uniform, and the electrical properties were expected to be poor. In particular, numbers of pores were found between the grains in 0.16 BST as shown in Figure 3e. Figure 3f shows the density of the fabricated (1−x)BNT–xBST ceramics. The theoretical density increases with the increase in BST composition because the theoretical density of BST (6.34 g/cm^3) is relatively larger than that of BNT (5.99 g/cm^3). As the composition of BST increased up to 0.12 BST, the density of the fabricated ceramics increased [28]. However, the density decreased at 0.14 BST, and the poorest density appeared at 0.16 BST. This represents the cracks and pores inside the ceramic identified in Figure 3e.

Figure 4 shows the frequency-dependent permittivity of (1−x)BNT–xBST ceramics at various compositions. At 1 kHz, 0.08 BST rose to 0.12 BST, and the permittivity increased from 905 to 1692, and as the BST composition increased to 0.16 BST, it was confirmed that the dielectric constant decreased to 444. Since the sintering temperature of BNT ceramics is lower than that of BST, it is not completely sintered as the composition of BST increases. It can be seen that the permittivity decreases again above 0.14 BST. Significantly, the decrease in permittivity in 0.16 BST seems to be due to the irregular grain size. This result shows that it can be expected that 0.12 BST is the best piezoelectric properties.

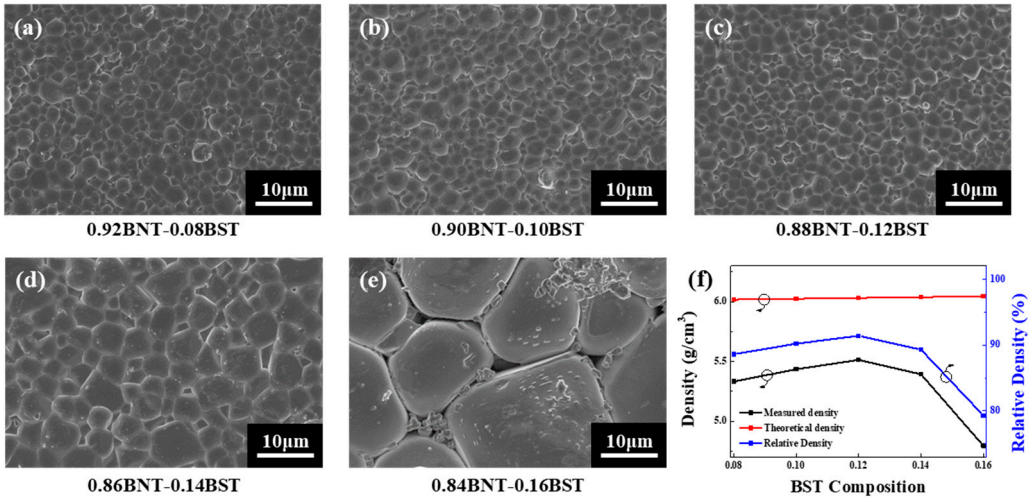

Figure 3. SEM images of (1−x)BNT–xBST ceramics according to BST composition with x = (**a**) 0.08, (**b**) 0.10, (**c**) 0.12, (**d**) 0.14, and (**e**) 0.16. (**f**) Density according to composition of fabricated ceramics.

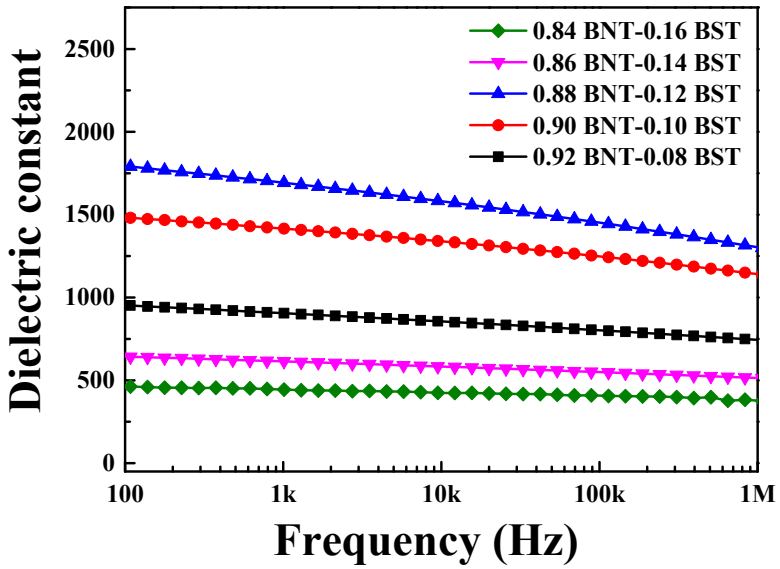

Figure 4. Variation in the frequency-dependent dielectric permittivity of (1−x)BNT–xBST ceramics according to the BST content in the frequency of 100 Hz to 1 MHz.

Figure 5 shows the polarization and field hysteresis curves of (1−x)BNT–xBST ceramics measured at a frequency of 60 Hz using the Sawyer–Tower method. It was confirmed that the remnant polarization increased as the BST composition increased to 0.12 BST [29,30]. At 0.12 BST, the saturation polarization (P_s), remanent polarization (P_r), and coercive electric field (E_c) were measured as 29.2 μC/cm^2, 23.3 μC/cm^2, and 19.9 kV/cm, respectively, and the hysteresis loop of typical piezoelectric ceramics was confirmed. A sharp decrease in P_r was confirmed at 0.14 BST. In 0.16 BST, the dielectric breakdown occurred due to leakage current, which was confirmed to be caused by a number of pores between grains, as shown in Figure 3e. As can be seen in the hysteresis loop of 0.14 BST, it changes to paraelectric [31].

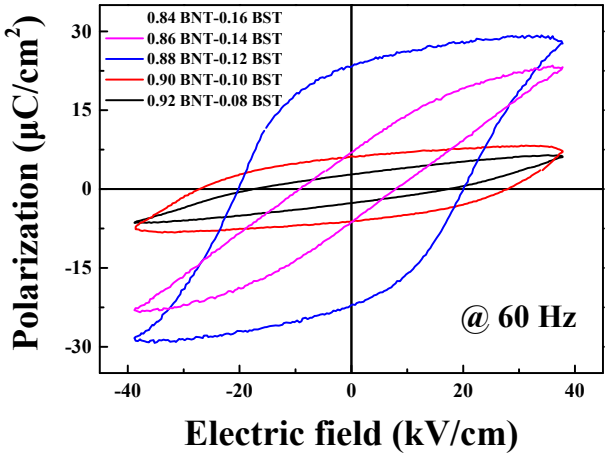

Figure 5. P-E hysteresis loop of (1−x)BNT–xBST ceramics according to the BST composition.

Figure 6a–d shows the resonance–antiresonance points measured for each composition. It can be seen that the resonance–antiresonance frequency increases as the BST composition increases. Figure 6e shows the measured piezoelectric charge coefficient and electromechanical coupling coefficient. Since the fabricated ceramic is a disk type, the electromechanical coupling coefficient (k_p) can be calculated and estimated using the following equation [32–34]:

$$k_p = \sqrt{2.51\frac{f_a - f_r}{f_a} - \left(\frac{f_a - f_r}{f_a}\right)^2}, \quad (3)$$

where f_a is the anti-resonant frequency and f_r is the resonant frequency. In 0.16 BST, the polarization process could not be performed due to leakage current. Figure 6e shows that the piezoelectric constant was confirmed to be excellent at 147 pC/N in 0.12 BST, and the electromechanical coupling coefficient was also confirmed with a maximum value of 0.375 for 0.12 BST. However, in 0.14 BST, d_{33} decreased to 80, while k_p decreased to 0.15. As shown in Figure 3c, the composition of (1−x)BNT–xBST ceramics was the most uniform and dense in 0.12 BST, and the highest piezoelectric properties were obtained.

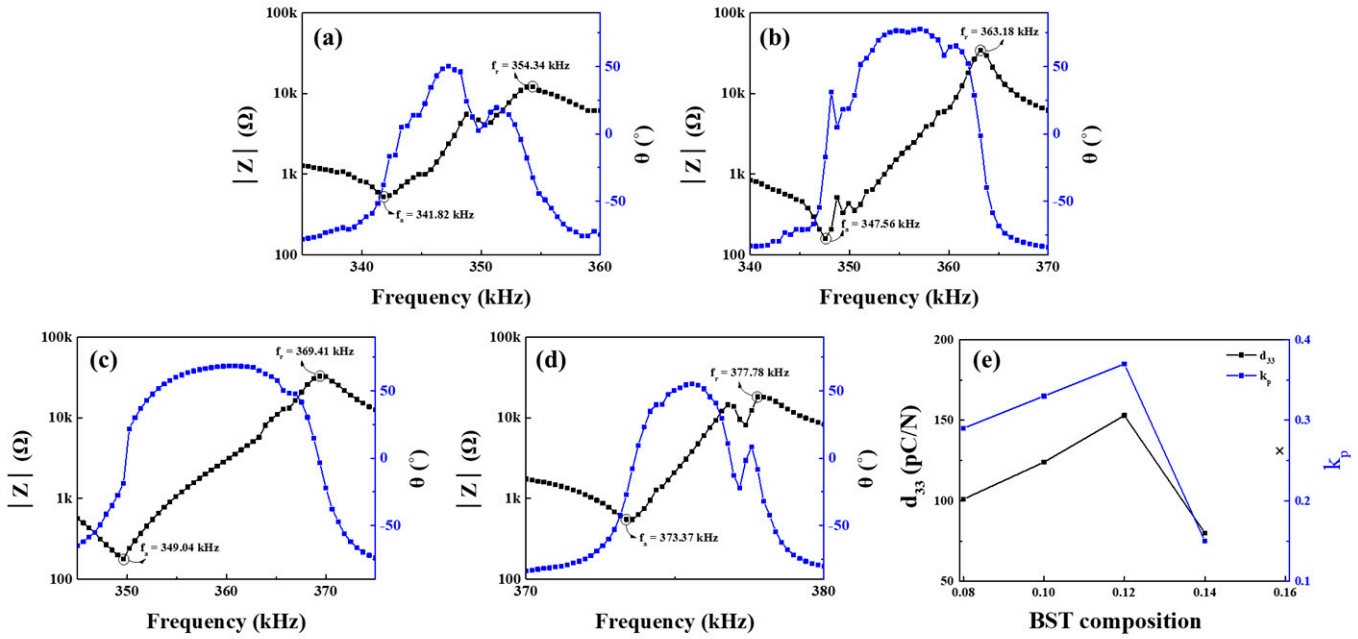

Figure 6. Electromechanical coupling coefficient of (1−x)BNT–xBST ceramics according to the BST composition (x = (**a**) 0.08, (**b**) 0.10, (**c**) 0.12, and (**d**) 0.14). (**e**) Variation in piezoelectric charge constant.

Figure 7 shows the temperature-dependent relative permittivity (ε_r) of (1−x)BNT–xBST (x = 0.08, 0.10, 0.12, 0.14, and 0.16) ceramics sintered at 1200 °C for 3 h. The (1−x)BNT–xBST ceramic samples showed Curie temperatures of 498, 476, 242, 237, and 222 °C for BST contents of 0.08, 0.10, 0.12, 0.14, and 0.16%, respectively. Table 1 shows the phase change and lattice parameter change according to the BST composition. According to X. Meng et al., it is known that the Curie temperature decreases when the tolerance factor increases. The formula to calculate this factor is as follows [35]:

$$\text{Tolerance factor, } t = \frac{r_A + r_O}{\sqrt{2}(r_B + r_O)} \quad (4)$$

where r_A is the radius of the A-site ion, r_B is the radius of the B-site ion, and r_O is the radius of the oxide ion at various BST compositions of (1−x)BNT–xBST ceramics. When the content of BST is increased, the content of Ba and Sr increases, and the tolerance factor increases [36,37]. This increased tolerance factor reduced the Curie temperature. T_m decreased compared to low-BST compositions but remained within 200 °C for all compositions.

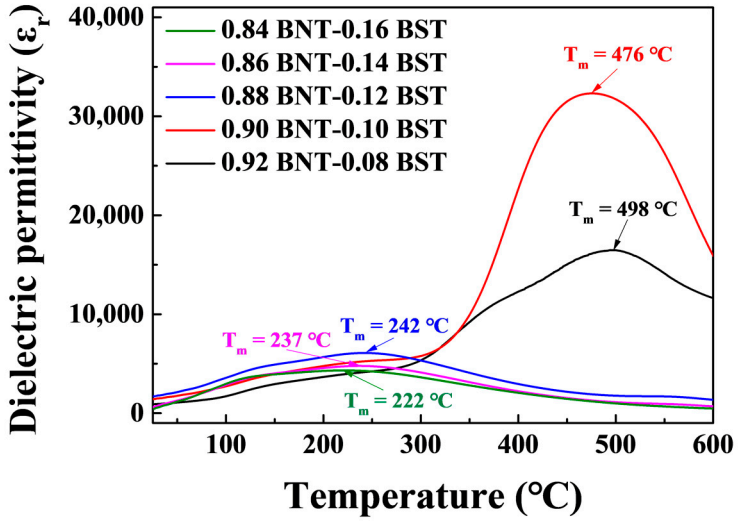

Figure 7. Temperature-dependent relative dielectric permittivity (ε_r) of (1−x)BNT–xBST ceramics sintered at 1200 °C for 3 h.

4. Conclusions

In this study, changes in properties were observed by adding 8 to 16 mol % of $(Ba_{0.5}Sr_{0.5})TiO_3$ to $(Bi_{0.5}Na_{0.5})TiO_3$-based piezoelectric ceramics. In 0.12 BST, the ratio of (200)/(002) was the highest. From there, it was confirmed that the grain size was also fine and that the crystal structure was dense. As the proportion of the BST composition increases to 12 mol %, due to the high-density microstructure, the dielectric constant was 1692, and the saturation polarization and remanent polarization were 29.2 μC/cm^2 and 23.3 μC/cm^2, respectively, indicating superior piezoelectric and electrical properties compared to other compositions. In addition, d_{33} was improved to 147 pC/N and k_p to 0.375. When the BST contents were increased, T_m was decreased in (1−x)BST–xBCT ceramics. However, T_m was observed above 200 °C for all compositions. Therefore, lead-based piezoelectric materials are expected to be replaced by lead-free $(1-x)(Bi_{0.5}Na_{0.5})TiO_3$–$x(Ba_{0.5}Sr_{0.5})TiO_3$ piezoelectric materials.

Author Contributions: Data curation, S.-J.K. and J.-H.K.; formal analysis, S.-M.K. and T.W.K.; investigation, T.W.K. and N.-H.K.; supervision, J.-H.K.; visualization, N.-H.K.; writing—original draft, S.-M.K. and J.-H.K.; writing—review and editing, T.W.K. and J.-H.K. All authors have read and agreed to the published version of the manuscript.

Funding: This work was supported by the Human Resources Development (No.20214000000280) of the Korea Institute of Energy Technology Evaluation and Planning (KETEP); grant funded by the Korean Government Ministry of Trade, Industry and Energy. Additionally, this research was supported by the MSIT (Ministry of Science and ICT), Korea, under the ITRC (Information Technology Research Center) support program (IITP-2022-2020-0-01655) supervised by the IITP (Institute of Information and Communications Technology Planning and Evaluation).

Institutional Review Board Statement: Not applicable.

Informed Consent Statement: Not applicable.

Data Availability Statement: The data presented in this study are available on request from the corresponding author.

Conflicts of Interest: The authors declare no conflict of interest.

References

1. Zhang, S.; Xia, R.; Shrout, T.R. Lead-free piezoelectric ceramics vs. PZT? *J. Electroceramics* **2007**, *19*, 251–257.
2. Hooker, M.W. Properties of PZT-Based Piezoelectric Ceramics Between −150 and 250 °C. *NASA* **1998**, *26*, 208708.
3. Panda, P.K.; Sahoo, B. PZT to lead free piezo ceramics: A review. *Ferroelectrics* **2015**, *474*, 128–143.
4. Chu, B.J.; Chen, D.R.; Li, G.R.; Yin, Q.R. Electrical properties of $Na_{1/2}Bi_{1/2}TiO_3$–$BaTiO_3$ ceramics. *J. Eur. Ceram. Soc.* **2002**, *22*, 2115–2121.
5. Yoshii, K.; Hiruma, Y.; Nagata, H.; Takenaka, T. Electrical properties and depolarization temperature of $(Bi_{1/2}Na_{1/2})$ TiO_3–$(Bi_{1/2}K_{1/2})$ TiO_3 lead-free piezoelectric ceramics. *Jpn. J. Appl. Phys.* **2006**, *45*, 4493.
6. Zhao, S.; Li, G.; Ding, A.; Wang, T.; Yin, Q. Ferroelectric and piezoelectric properties of $(Na, K)_{0.5}Bi_{0.5}TiO_3$ lead free ceramics. *J. Phys. D Appl. Phys.* **2006**, *39*, 2277.
7. Takenaka, T.; Maruyama, K.I.M.K.I.; Sakata, K.S.K. $(Bi_{1/2}Na_{1/2})TiO_3$–$BaTiO_3$ system for lead-free piezoelectric ceramics. *Jpn. J. Appl. Phys.* **1991**, *30*, 2236. [CrossRef]
8. Kwon, Y.H.; Shin, D.J.; Lee, G.H.; Koh, J.H. Sintering temperature dependent piezoelectric properties of (Bi,Na)TiO_3–(Ba,Sr) TiO_3 ceramics. *Ceram. Int.* **2016**, *42*, 10422–10427.
9. Nguyen, M.D.; Trinh, T.Q.; Dekkers, M.; Houwman, E.P.; Vu, H.N.; Rijnders, G. Effect of dopants on ferroelectric and piezoelectric properties of lead zirconate titanate thin films on Si substrates. *Ceram. Int.* **2014**, *40*, 1013–1018.
10. Lin, D.; Kwok, K.W.; Chan, H.L.W. Structure and electrical properties of $Bi_{0.5}Na_{0.5}TiO_3$–$BaTiO_3$–$Bi_{0.5}Li_{0.5}TiO_3$ lead-free piezoelectric ceramics. *Solid State Ion.* **2008**, *178*, 1930–1937.
11. Wang, X.X.; Tang, X.G.; Chan, H.L.W. Electromechanical and ferroelectric properties of $(Bi_{1/2}Na_{1/2})$ TiO_3–$(Bi_{1/2}K_{1/2})TiO_3$–$BaTiO_3$ lead-free piezoelectric ceramics. *Appl. Phys. Lett.* **2004**, *85*, 91–93.
12. Shieh, J.; Wu, K.C.; Chen, C.S. Switching characteristics of MPB compositions of $(Bi_{0.5}Na_{0.5})TiO_3$–$BaTiO_3$–$(Bi_{0.5}K_{0.5})TiO_3$ lead-free ferroelectric ceramics. *Acta Mater.* **2007**, *55*, 3081–3087.
13. Makiuchi, Y.; Aoyagi, R.; Hiruma, Y.; Nagata, H.; Takenaka, T. $(Bi_{1/2}Na_{1/2})TiO_3$–$(Bi_{1/2}K_{1/2})TiO_3$–$BaTiO_3$-based lead-free piezoelectric ceramics. *Jpn. J. Appl. Phys.* **2005**, *44*, 4350. [CrossRef]
14. Li, Y.; Chen, W.; Xu, Q.; Zhou, J.; Gu, X.; Fang, S. Electromechanical and dielectric properties of $Na_{0.5}Bi_{0.5}TiO_3$–$K_{0.5}Bi_{0.5}TiO_3$–$BaTiO_3$ lead-free ceramics. *Mater. Chem. Phys.* **2005**, *94*, 328–332. [CrossRef]
15. Li, Z.; Li, D.X.; Shen, Z.Y.; Zeng, X.; Song, F.; Luo, W.; Li, Y. Remarkably enhanced dielectric stability and energy storage properties in BNT—BST relaxor ceramics by A-site defect engineering for pulsed power applications. *J. Adv. Ceram.* **2022**, *11*, 283–294.
16. Li, D.; Shen, Z.Y.; Li, Z.; Luo, W.; Wang, X.; Wang, Z.; Li, Y. PE hysteresis loop going slim in $Ba_{0.3}Sr_{0.7}TiO_3$-modified $Bi_{0.5}Na_{0.5}TiO_3$ ceramics for energy storage applications. *J. Adv. Ceram.* **2020**, *9*, 183–192.
17. Li, D.; Shen, Z.Y.; Li, Z.; Wang, X.; Luo, W.Q.; Song, F.; Li, Y. Structural evolution, dielectric and ferroelectric properties of $(1-x)Bi_{0.5}Na_{0.5}TiO_3$–$xBa_{0.3}Sr_{0.7}TiO_3$ ceramics. *J. Mater. Sci. Mater. Electron.* **2019**, *30*, 5917–5922.
18. Yoshimura, T.; Fujimura, N. Polarization Hysteresis Loops of Ferroelectric Gate Capacitors Measured by Sawyer-Tower Circuit. *Jpn. J. Appl. Phys.* **2003**, *42*, 6011–6014.
19. Zhang, L.; Wang, X.; Yang, W.; Liu, H.; Yao, X. Structure and relaxor behavior of $BaTiO_3$–$CaTiO_3$–$SrTiO_3$ ternary system ceramics. *J. Appl. Phys.* **2008**, *104*, 014104. [CrossRef]
20. Cui, Y.; Liu, X.; Jiang, M.; Zhao, X.; Shan, X.; Li, W.; Zhou, C. Lead-free $(Ba_{0.85}Ca_{0.15})(Ti_{0.9}Zr_{0.1})O_3$–$CeO_2$ ceramics with high piezoelectric coefficient obtained by low-temperature sintering. *Ceram. Int.* **2012**, *38*, 4761–4764. [CrossRef]
21. Li, Z.Y.; Lam, W.M.; Yang, C.; Xu, B.; Ni, G.X.; Abbah, S.A.; Cheung, K.M.C.; Luk, K.D.K.; Lu, W.W. Chemical composition, crystal size and lattice structural changes after incorporation of strontium into biomimetic apatite. *Biomaterials* **2007**, *28*, 1452–1460. [CrossRef]
22. Zawrah, M.F. Investigation of lattice constant, sintering and properties of nano Mg–Al spinels. *Mater. Sci. Eng. A* **2004**, *382*, 362–370. [CrossRef]
23. Lee, H.W.; Moon, S.; Choi, C.H.; Kim, D.K. Synthesis and size control of tetragonal barium titanate nanopowders by facile solvothermal method. *J. Am. Ceram. Soc.* **2012**, *95*, 2429–2434.

24. Joshi, U.A.; Yoon, S.; Baik, S.; Lee, J.S. Surfactant-free hydrothermal synthesis of highly tetragonal barium titanate nanowires: A structural investigation. *J. Phys. Chem. B* **2006**, *110*, 12249–12256. [CrossRef]
25. Jiang, J.; Meng, X.; Li, L.; Guo, S.; Huang, M.; Zhang, J.; Zhang, S.T. Ultrahigh energy storage density in lead-free relaxor antiferroelectric ceramics via domain engineering. *Energy Storage Mater.* **2021**, *43*, 383–390. [CrossRef]
26. Boonlakhorn, J.; Thongbai, P. Dielectric properties, nonlinear electrical response and microstructural evolution of $CaCu_3Ti_{4-x}Sn_xO_{12}$ ceramics prepared by a double ball-milling process. *Ceram. Int.* **2020**, *46*, 4952–4958.
27. Thongbai, P.; Yamwong, T.; Maensiri, S.; Amornkitbamrung, V.; Chindaprasirt, P. Improved dielectric and nonlinear electrical properties of fine-grained $CaCu_3Ti_4O_{12}$ ceramics prepared by a glycine-nitrate process. *J. Am. Ceram. Soc.* **2014**, *97*, 1785–1790.
28. Jain, A.; Panwar, A.K.; Saroha, R.; Jha, A.K. Enhanced structural, dielectric, ferroelectric, and piezoelectric properties of $(1-x)Ba_{0.9}Sr_{0.1}TiO_3$–$(x)Ba_{0.7}Ca_{0.3}TiO_3$ ceramics derived using mechano-chemical activation technique. *J. Am. Ceram. Soc.* **2017**, *100*, 5239–5248.
29. Qi, W.; Cao, J.; Li, Z.; Wang, Y. Effect of Sr doping on the energy storage properties of BNT–BST–KNN anti-ferroelectric ceramics. *Ferroelectrics* **2021**, *577*, 229–235. [CrossRef]
30. Henaish, A.M.; Mostafa, M.; Weinstein, I.; Hemeda, O.; Salem, B. Ferroelectric and Dielectric Properties of Strontium Titanate Doped with Barium. *Magnetism* **2021**, *1*, 22–36.
31. Lee, J.S.; Yoon, S.; Lim, J.H.; Park, C.K.; Ryu, J.; Jeong, D.Y. Improvement of Energy Storage Characteristics of $(Ba_{0.7}Ca_{0.3})TiO_3$ Thick Films by the Increase of Electric Breakdown Strength from Nano-Sized Grains. *Korean J. Mater. Res.* **2019**, *29*, 73–78. [CrossRef]
32. Erhart, J.; Sebastian, T. Effective electromechanical coupling for the partially electroded ceramic resonators different geometries. *Ann. "Dunarea Jos" Univ. Fascicle IX Metall. Mater. Sci.* **2015**, *38*, 7–16.
33. Yamashita, Y.; Harada, K.; Hosono, Y.; Natsume, S.; Ichinose, N. Effects of B-site ions on the electromechanical coupling factors of $Pb(B'B'')O_3$–$PbTiO_3$ piezoelectric materials. *Jpn. J. Appl. Phys.* **1998**, *37*, 5288.
34. Chen, F.; Kong, L.; Song, W.; Jiang, C.; Tian, S.; Yu, F.; Zhao, X. The electromechanical features of $LiNbO_3$ crystal for potential high temperature piezoelectric applications. *J. Mater.* **2019**, *5*, 73–80. [CrossRef]
35. Meng, X.; Chen, Q.; Fu, H.; Liu, H.; Zhu, J. Influence of PNN on the structure and electronic properties of BSPT ceramics. *J. Mater. Sci. Mater. Electron.* **2018**, *29*, 12785–12794.
36. Wang, Y.; Cao, J.; Li, Z. Effects of co-doping of Sr element and KNN group on the dielectric properties of BNT-BT ceramics. *Ferroelectrics* **2021**, *573*, 166–172. [CrossRef]
37. Wu, R.; Huang, L.; Jin, L.; Gao, R.; Bai, L.; Xu, Z. Microstructure, dielectric and ferroelectric properties of $(1-x)Bi_{0.5}Na_{0.5}TiO_3$–$x(0.8Ba_{0.9}Sr_{0.1}TiO_3$–$0.2BiFeO_3)$ lead-free ceramics. *J. Mater. Sci. Mater. Electron.* **2022**, *33*, 25404–25418. [CrossRef]